

## Out-of-plane Piezoelectricity and Ferroelectricity in Layered #InSe Nano-flakes

Yu Zhou, Di Wu, Yihan Zhu, Yujin Cho, Qing He, Xiao Yang, Kevin Herrera, Zhaodong Chu, Yu Han, Mike Downer, Hailin Peng, and Keji Lai

*Nano Lett.*, **Just Accepted Manuscript** • DOI: 10.1021/acs.nanolett.7b02198 • Publication Date (Web): 25 Aug 2017

Downloaded from <http://pubs.acs.org> on August 29, 2017

### Just Accepted

“Just Accepted” manuscripts have been peer-reviewed and accepted for publication. They are posted online prior to technical editing, formatting for publication and author proofing. The American Chemical Society provides “Just Accepted” as a free service to the research community to expedite the dissemination of scientific material as soon as possible after acceptance. “Just Accepted” manuscripts appear in full in PDF format accompanied by an HTML abstract. “Just Accepted” manuscripts have been fully peer reviewed, but should not be considered the official version of record. They are accessible to all readers and citable by the Digital Object Identifier (DOI®). “Just Accepted” is an optional service offered to authors. Therefore, the “Just Accepted” Web site may not include all articles that will be published in the journal. After a manuscript is technically edited and formatted, it will be removed from the “Just Accepted” Web site and published as an ASAP article. Note that technical editing may introduce minor changes to the manuscript text and/or graphics which could affect content, and all legal disclaimers and ethical guidelines that apply to the journal pertain. ACS cannot be held responsible for errors or consequences arising from the use of information contained in these “Just Accepted” manuscripts.



# Out-of-plane Piezoelectricity and Ferroelectricity in Layered $\alpha$ - $\text{In}_2\text{Se}_3$ Nano-flakes

Yu Zhou<sup>1+</sup>, Di Wu<sup>2+</sup>, Yihan Zhu<sup>3</sup>, Yujin Cho<sup>2</sup>, Qing He<sup>4</sup>, Xiao Yang<sup>1</sup>, Kevin Herrera<sup>2</sup>, Zhaodong Chu<sup>2</sup>, Yu Han<sup>3</sup>, Michael C. Downer<sup>2</sup>, Hailin Peng<sup>1\*</sup> and Keji Lai<sup>2\*</sup>

<sup>1</sup>College of Chemistry and Molecular Engineering, Peking University, Beijing 100871, China

<sup>2</sup>Department of Physics, University of Texas at Austin, Austin TX 78712, USA

<sup>3</sup>Physical Sciences and Engineering Division, King Abdullah University of Science and Technology, Thuwal 23955-6900, Saudi Arabia

<sup>4</sup>Department of Physics, Durham University, Durham DH1 3LE, United Kingdom

**ABSTRACT:** Piezoelectric and ferroelectric properties in the two dimensional (2D) limit are highly desired for nanoelectronic, electromechanical, and optoelectronic applications. Here we report the first experimental evidence of out-of-plane piezoelectricity and ferroelectricity in van der Waals layered  $\alpha$ - $\text{In}_2\text{Se}_3$  nano-flakes. The non-centrosymmetric R3m symmetry of the  $\alpha$ - $\text{In}_2\text{Se}_3$  samples is confirmed by scanning transmission electron microscopy, second-harmonic generation, and Raman spectroscopy measurements. Domains with opposite polarizations are visualized by piezo-response force microscopy. Single-point poling experiments suggest that the polarization is potentially switchable for  $\alpha$ - $\text{In}_2\text{Se}_3$  nano-flakes with thicknesses down to  $\sim 10$  nm. The piezotronic effect is demonstrated in two-terminal devices, where the Schottky barrier can be modulated by the strain-induced piezopotential. Our work on polar  $\alpha$ - $\text{In}_2\text{Se}_3$ , one of the model 2D piezoelectrics and ferroelectrics with simple crystal structures, shows its great potential in electronic and photonic applications.

**KEYWORDS:**  $\text{In}_2\text{Se}_3$ , 2D materials, piezoelectric, ferroelectric, polarization

1  
2  
3  
4  
5  
6  
7  
8  
9  
10  
11  
12  
13  
14  
15  
16  
17  
18  
19  
20  
21  
22  
23  
24  
25  
26  
27  
28  
29  
30  
31  
32  
33  
34  
35  
36  
37  
38  
39  
40  
41  
42  
43  
44  
45  
46  
47  
48  
49  
50  
51  
52  
53  
54  
55  
56  
57  
58  
59  
60

Two-dimensional (2D) van der Waals (vdW) materials encompassing a broad range of novel electronic,<sup>1, 2</sup> magnetic,<sup>3</sup> thermal,<sup>4, 5</sup> and optical properties<sup>6, 7</sup> have attracted substantial research interest over the past decade, promising the development of next-generation multi-functional devices. Among various functionalities, piezoelectricity and ferroelectricity widely exploited for the applications in memories,<sup>8</sup> capacitors,<sup>9</sup> actuators<sup>10</sup> and sensors<sup>11</sup> are relatively scarce in 2D materials. In 2H-stacking transitional metal dichalcogenides (TMDs) such as MoS<sub>2</sub>, the inversion symmetry in bulk crystals is broken in ultrathin flakes with odd number of layers, leading to the in-plane piezoelectricity that has been theoretically predicted and experimentally demonstrated<sup>12-14</sup>. Recently, spontaneous in-plane polarization has also been reported in monolayer group IV monochalcogenides<sup>15-17</sup>. However, in device applications, out-of-plane piezoelectricity and ferroelectricity are more straightforward for circuit designs. To date, CuInP<sub>2</sub>S<sub>6</sub> remains the only known vdW ferroelectric with out-of-plane polarization, although the crystal structure is rather complicated and the polarization is only switchable for films above 4 nm<sup>18-21</sup>. Since traditional ultrathin ferroelectric films such as PbTiO<sub>3</sub> and BaTiO<sub>3</sub> are plagued by dangling bonds and dead layers at the ferroelectric/metal interfaces<sup>9</sup>, it is of great interest to explore new out-of-plane polarized 2D ferroelectrics for non-volatile memory and photovoltaic applications, as well as to enable 2D vdW heterostructures with novel functionalities<sup>22-25</sup>.

2D out-of-plane ferroelectricity is highly nontrivial, as the depolarization field due to the lack of screening charges may strongly suppress spontaneous polarization in vdW materials. In a recent report, Ding et al. predicted that the layered semiconducting indium selenide ( $\alpha$ -In<sub>2</sub>Se<sub>3</sub>) is a room-temperature out-of-plane polarized ferroelectric down to the single-layer limit (thickness  $\sim$  1 nm), with a calculated electric dipole of 0.11 eÅ/unit cell<sup>26</sup>. In<sub>2</sub>Se<sub>3</sub> has been widely explored for phase-change memory, thermoelectric, and photoelectric applications.<sup>27, 28</sup> Owing to its

1  
2  
3 polymorphism and complicated phase diagram, however, even the crystal structure of the  
4 thermodynamically stable phase at the room temperature (commonly denoted as  $\alpha$ - $\text{In}_2\text{Se}_3$ )  
5 remains controversial.<sup>29-31</sup> Here we report the first experimental observation of out-of-plane  
6 piezoelectricity and ferroelectricity in multi-layer  $\alpha$ - $\text{In}_2\text{Se}_3$ . Using a combination of transmission  
7 electron microscopy (TEM), second-harmonic generation, Raman spectroscopy, and piezo-force  
8 microcopy (PFM), we show that our  $\text{In}_2\text{Se}_3$  samples exhibit the rhombohedral R3m structure (Fig.  
9 1a), which is non-centrosymmetric and supports the presence of a spontaneous polarization that  
10 is potentially switchable by an external bias. The piezotronic effect is demonstrated in that the  
11 charge transport in a prototypical device can be modulated by the piezoelectricity. Our work  
12 highlights the potential of 2D piezoelectric and ferroelectric materials for novel applications such  
13 as sensors, flexible electronics, and nano-electromechanical systems.  
14  
15  
16  
17  
18  
19  
20  
21  
22  
23  
24  
25  
26  
27  
28  
29

30 In this study,  $\text{In}_2\text{Se}_3$  nano-flakes prepared by mechanical exfoliation onto conducting  
31 substrates and vapor-phase deposition (VPD) on flexible mica substrates are both studied<sup>32</sup>. Both  
32 types of samples have undergone a slow thermal annealing process before the characterizations  
33 (see Methods). In order to elucidate the out-of-plane structure of these nano-flakes, we use  
34 aberration corrected scanning transmission electron microscopy (AC-STEM) to directly image  
35 the cross sections of VPD-grown multi-layer nano-flakes. As shown in Fig. 1b, the cross-  
36 sectional samples are fabricated by focused-ion beam (FIB) cutting along the [120] and [100]  
37 axes of  $\text{In}_2\text{Se}_3$  nano-flakes, respectively. From the annular bright-field (ABF) STEM image taken  
38 on the [120] cross-section (Fig.1c), the vdW gaps (in bright contrast) are clearly visible between  
39 the Se(1)-In(2)-Se(3)-In(4)-Se(5) quintuple layers. Interestingly, the ABF-STEM intensity  
40 profile in Fig. 1d indicates that the Se(3) atom is shifted off-center towards the neighboring In(2)  
41 atom, which breaks the inversion symmetry of each quintuple layer and gives rise to an out-of-  
42  
43  
44  
45  
46  
47  
48  
49  
50  
51  
52  
53  
54  
55  
56  
57  
58  
59  
60

1  
2  
3 plane dipole. This observation is consistent with the theoretical calculation<sup>26</sup>. The high angle  
4 annular dark field (HAADF) image and the ABF image along the [100] direction are shown in  
5  
6  
7  
8  
9  
10  
11  
12  
13  
14  
15  
16  
17  
18  
19  
20  
21  
22  
23  
24  
25  
26  
27  
28  
29  
30  
31  
32  
33  
34  
35  
36  
37  
38  
39  
40  
41  
42  
43  
44  
45  
46  
47  
48  
49  
50  
51  
52  
53  
54  
55  
56  
57  
58  
59  
60

plane dipole. This observation is consistent with the theoretical calculation<sup>26</sup>. The high angle annular dark field (HAADF) image and the ABF image along the [100] direction are shown in Supplementary Information Fig. S1. The STEM images and structural analysis suggest that the crystal structure of our In<sub>2</sub>Se<sub>3</sub> nano-flakes follows the R3m symmetry<sup>33,34</sup>. We note that  $\alpha$ -In<sub>2</sub>Se<sub>3</sub> samples in the R-3m or P6<sub>3</sub>/mmc symmetry groups have also been reported in the literature<sup>28,30,35</sup>. While the origin of this discrepancy is not clear and may subject to future investigations, it is possible that the slow annealing pre-treatment is responsible for the polar structure observed in our samples.

The symmetry of our  $\alpha$ -In<sub>2</sub>Se<sub>3</sub> flakes is further explored by optical second-harmonic generation (SHG). Here a Ti: Sapphire femtosecond-pulsed laser with wavelength  $\lambda_{\text{ex}} = 798$  nm generates second-harmonic (SH) signals in reflection. Figure 2a compares the SH spectral intensity ( $\lambda = 399$  nm, all polarizations) generated by s-polarized incident laser from a vapor-phase deposited thin flake (thickness  $t = 2$  nm) with the 10-fold stronger SH peak that an identical pulse generates from an exfoliated thick flake ( $t \sim 100$  nm). These SH signals are, respectively,  $\sim 70$  and  $\sim 350$  times stronger than an identical pulse generates in reflection from a 2 nm thick GaAs film. Moreover, s-polarized SHG (Figure 2b), which has no contribution from the surface, is nearly as strong (averaged over azimuthal angles) as the p-polarized signal (Figure 2c), for which a surface contribution is allowed in principle. Note that VPD grown flakes with thickness from monolayer to four-layer all exhibit prominent SHG intensity (Fig. S3). These observations show that the SHG signal originates from the non-centrosymmetric bulk  $\alpha$ -In<sub>2</sub>Se<sub>3</sub> crystal, rather than from the broken inversion symmetry at the surface<sup>36</sup>. The result differs significantly from that of layered MoS<sub>2</sub>, where SH intensities are negligible in even-layer and bulk samples due to the restoration of inversion symmetry<sup>37,38</sup>. The azimuthal angle dependence

1  
2  
3 of the SHG intensity is also measured on the VPD sample. For the R3m symmetry, SHG  
4 intensities take the form  $I$  (s-in/s-out) =  $I_0 \cos^2(3\theta)$  and  $I$  (s-in/p-out) =  $I_0 (A+B \cdot \cos(3\theta))^2$  in each  
5 polarization configuration. Here  $\theta$  is the azimuthal angle from [120] direction, and  $I_0$ , A, and B  
6 are constants determined by Fresnel coefficients and the nonlinear susceptibility tensor. As  
7 shown in Figs. 2b and 2c, the calculated responses fit well to the s-(Figure 2b) and p-polarized  
8 (Figure 2c) SHG data in each configuration. In s-in/s-out configuration, only one component of  
9 the susceptibility tensor,  $\chi_{yyy}$ , generates the SH signal; in s-in/p-out configuration, the out-of-  
10 plane component,  $\chi_{zyy}$ , also contributes to the signal. The SHG data are therefore consistent with  
11 the conclusion that the symmetry group of our  $\alpha$ -In<sub>2</sub>Se<sub>3</sub> crystals is R3m.  
12  
13  
14  
15  
16  
17  
18  
19  
20  
21  
22  
23  
24

25 The broken inversion symmetry and polar structure in In<sub>2</sub>Se<sub>3</sub> do not ensure its  
26 ferroelectricity, which necessarily requires the presence of a spontaneous polarization that is  
27 switchable under external electric fields. In order to investigate the piezoelectricity and  
28 ferroelectricity of the  $\alpha$ -In<sub>2</sub>Se<sub>3</sub> samples, PFM measurements (see Methods) have been carried out.  
29 Figure 3a shows the atomic force microscopy (AFM) image of a thick (> 100 nm) exfoliated  
30 In<sub>2</sub>Se<sub>3</sub> flake with atomically smooth terraces. The out-of-plane PFM phase and amplitude images  
31 in Fig. 3b and 3c show two distinct regions with 180° phase difference, corresponding to  
32 domains with up and down polarization vectors perpendicular to the flake surface; whereas the  
33 domain walls appear as darker lines in the PFM amplitude image (Fig. 3c). Thinner flakes with  
34 thicknesses ranging from 3 nm to 60 nm (Fig. 3d) are also exfoliated onto gold substrates for  
35 PFM studies. As shown in Figs. 3e and 3f, clear out-of-plane domains can be observed. It is  
36 worth noting that some but not all of the domain walls coincide with the location of the flake  
37 edges, which suggests that the PFM phase contrasts are more likely coming from real  
38 polarization contribution rather than other artifacts between different layers. Unlike CuInP<sub>2</sub>S<sub>6</sub>,  
39  
40  
41  
42  
43  
44  
45  
46  
47  
48  
49  
50  
51  
52  
53  
54  
55  
56  
57  
58  
59  
60

1  
2  
3 the  $\text{In}_2\text{Se}_3$  flake does not display an obvious thickness dependence on the PFM amplitude  
4 contrast, which is consistent with the theoretical calculations<sup>27</sup>. To rule out the possibility that the  
5 PFM contrast is caused by the coexistence of different phases, local Raman spectroscopy is  
6 performed in this sample at different locations (marked with numerical labels in Fig. 3e), with  
7 the corresponding Raman spectra shown in Fig. 3g. Three prominent peaks, A(LO+TO) mode at  
8  $104\text{ cm}^{-1}$  and A(LO) mode at  $182$  and  $203\text{ cm}^{-1}$ , can be observed at locations 2-6. (Note that the  
9 regions with  $t = 3\text{ nm}$  might have been oxidized by the Raman excitation laser.) The Raman  
10 frequencies are distinctly different from those of another room-temperature stable phase ( $\beta$   
11 phase), with A(LO+TO), A(TO), and A(LO) Raman modes centered at  $\sim 110\text{ cm}^{-1}$ ,  $\sim 175\text{ cm}^{-1}$  and  
12  $\sim 205\text{ cm}^{-1}$ , respectively<sup>30, 39</sup>. In accordance with previous Raman work,<sup>31</sup> the presence of the  
13 A(LO) mode indicates a lack of inversion symmetry in the R3m structure, consistent with the  
14 aforementioned STEM and SHG data.  
15  
16  
17  
18  
19  
20  
21  
22  
23  
24  
25  
26  
27  
28  
29  
30  
31

32 We have also performed PFM tip poling experiments to study the ferroelectric hysteresis  
33 behavior of  $\alpha\text{-In}_2\text{Se}_3$ . Unfortunately, due to the small bulk resistivity, significant leakage current  
34 usually takes place before the switching events across the entire sample. Fig. S4 shows the I-V  
35 characteristics across a 15-nm-thick  $\text{In}_2\text{Se}_3$  flake between a  $1\text{ }\mu\text{m} \times 1\text{ }\mu\text{m}$  Au pad and the bottom  
36 electrode. Substantial leakage current is observed for a bias beyond  $\pm 3\text{ V}$ , indicative of a large  
37 amount of defects (most likely Se vacancies) and charge carriers in the material. Because of the  
38 charge screening, we are not able to demonstrate the conventional remnant P-E hysteresis loop  
39 by the Sawyer-Tower method<sup>40</sup>. Nevertheless, we show that it is possible to obtain bias-on PFM  
40 hysteresis loops at individual points of the  $\text{In}_2\text{Se}_3$  flakes. An example on a 20-nm-thick sample is  
41 seen in Figs. 4a and 4b, where a stiff cantilever with a spring constant of  $40\text{ N/m}$  is used and the  
42 DC bias voltage is swept between  $-3\text{ V}$  and  $+6\text{ V}$  with an AC voltage of  $800\text{ mV}$ . Here the  
43  
44  
45  
46  
47  
48  
49  
50  
51  
52  
53  
54  
55  
56  
57  
58  
59  
60

1  
2  
3 amplitude response shows a butterfly loop with an opening of  $\sim 1.5$  V, whereas the phase  
4 switches  $180^\circ$  at the same turning points. The unsaturated amplitude signal is likely due to the  
5 significant leakage (high concentration of free carriers) of the samples, although we cannot  
6 exclude the possibility of surface charging effect. The offset of the loop from zero bias is from  
7 the Schottky barrier difference between the upper ( $\text{In}_2\text{Se}_3$  / IrPt tip) and lower ( $\text{In}_2\text{Se}_3$  / Au  
8 substrate) surfaces of the sample. Similar results are acquired on flakes with thicknesses down to  
9  $\sim 10$  nm and the data resemble the hysteresis loops in standard ferroelectrics like PZT (Fig. S5).  
10 We emphasize that this extrinsic leakage effect may be mitigated by doping of the opposite type  
11 of charged impurities or using a different growth mechanism such as molecular-beam epitaxy  
12 (MBE). The same practice, for instance, has been successfully adopted to suppress bulk carriers  
13 in the  $\text{Bi}_2\text{Se}_3$  family of topological insulators<sup>41, 42</sup>.  
14  
15  
16  
17  
18  
19  
20  
21  
22  
23  
24  
25  
26  
27  
28  
29

30 Finally, a flexible  $\text{In}_2\text{Se}_3$  device taking advantage of its out-of-plane piezoelectricity was  
31 demonstrated in Fig. 5. Standard photolithography is used to fabricate two-terminal devices on  
32 the VPD-grown multi-layer  $\text{In}_2\text{Se}_3$  flakes ( $\sim 10$  nm) on mica substrates. High work-function metal  
33 Pd (20 nm) are deposited on the sample surface to form Schottky contacts. As shown in Fig. 5a,  
34 the source-drain current increases (decreases) considerably when the  $\text{In}_2\text{Se}_3$  flake is under a small  
35 tensile (compressive) strain of  $\pm 0.1\%$ . Such a piezotronic effect has been previously reported in  
36 zinc oxide thin films<sup>43</sup>, where the Schottky barrier height is modulated by the bound charges  
37 induced by the piezoelectricity of the semiconducting material, as schematically illustrated in  
38 Figs. 5b – 5e. Fifteen 2D  $\text{In}_2\text{Se}_3$  devices have been investigated and all display the same transport  
39 characteristics in our experiment, suggesting a robust piezotronic effect that can be utilized for  
40 electromechanical energy transduction applications.  
41  
42  
43  
44  
45  
46  
47  
48  
49  
50  
51  
52  
53  
54  
55  
56  
57  
58  
59  
60



1  
2  
3 To summarize, the out-of-plane piezoelectricity and ferroelectricity in multi-layer  $\alpha$ -  
4  $\text{In}_2\text{Se}_3$  are explored by a combination of structural, optical, and electrical characterizations. The  
5  
6 non-centrosymmetric  $R3m$  crystal symmetry is confirmed by STEM, SHG, and Raman  
7  
8 measurements. Ferroelectric domains are clearly visualized by PFM and the out-of-plane  
9  
10 polarization is potentially switchable in samples with  $\sim 10$  nm of thickness. Finally, the  
11  
12 modulation of charge transport by bending of the substrate has also been demonstrated with a  
13  
14 flexible device with mica substrate, showing great potential for applications in nanoscale  
15  
16 electromechanical devices and piezotronic sensors. With further reduction of the bulk carrier  
17  
18 density, it is possible that ferroelectric  $\text{In}_2\text{Se}_3$  can be realized down to the single layer limit,  
19  
20 which is highly desirable for memory, sensing, and photovoltaic applications.  
21  
22  
23  
24  
25  
26  
27  
28  
29

## 30 Methods

31  
32 *Sample preparation.*  $\text{In}_2\text{Se}_3$  nano-flakes were grown on flexible fluorophlogopite mica substrates  
33  
34 via vdW epitaxy in a pressure controllable vapor deposition system equipped with a 1-inch  
35  
36 quartz tube.<sup>32</sup> The  $\text{In}_2\text{Se}_3$  powder source (99.99%, Alfa Aesar) was heated to 690-750 °C at the  
37  
38 center of the tube furnace. The vapor was transported downstream by  $\sim 50$  sccm Ar gas with  
39  
40 pressure controlled at  $\sim 50$  torr. The growth of  $\text{In}_2\text{Se}_3$  nano-flakes occurred on the mica substrates  
41  
42 placed 7-12 cm away from the heated center. After growth, the chamber was naturally cooled  
43  
44 down to room temperature. Thin flakes were also exfoliated onto Au surface from the bulk taken  
45  
46 out of the growth chamber for PFM measurements.  
47  
48  
49  
50

51  
52 *STEM.* The cross-section TEM samples were prepared by focused ion beam cutting from two  
53  
54 directions and were characterized by an aberration-corrected and monochromated G2 cubed  
55  
56 Titan 60-300 electron microscope under 60 kV.  
57  
58  
59  
60

1  
2  
3 *SHG microscopy.* A continuous-wave Ti: Sapphire laser operating at  $\sim 798$  nm, 76 MHz  
4 repetition rate, 150 fs pulse duration with *s*-polarization were focused on the sample surface at  
5  
6 incident angle  $\theta = 45^\circ$ , and SHG signals with *s* or *p*-polarization were collected in a reflection  
7  
8 geometry. A photo-multiplier tube (PMT) with bandpass filters was used to suppress the  
9  
10 fundamental wave. It was confirmed that SHG signals scaled quadratically with the incident  
11  
12 fundamental intensity.  
13  
14  
15

16  
17  
18 *PFM measurements.* PFM measurements were conducted using a Park XE-70 system equipped  
19  
20 with a Zurich HF2LI lock-in amplifier. P-E hysteresis loops were obtained with Asylum  
21  
22 Research MFP-3D Infinity. Using stiff cantilevers with a spring constant of 40 N/m were used to  
23  
24 eliminate the electrostatic contribution.  
25  
26

27  
28 *Raman spectroscopy characterization.* Raman spectroscopy was carried out using Witec Alpha  
29  
30 300 micro-Raman confocal microscope with a 488 nm laser excitation. The laser power was  
31  
32 minimized to avoid burning the flakes.  
33  
34

35  
36 *Device fabrication and measurements.* The flexible  $\text{In}_2\text{Se}_3$  two-terminal devices were achieved  
37  
38 by standard photolithography process, electron-beam deposition of Pd/Au (20 nm/50 nm) and  
39  
40 gold wire pasted by silver epoxy for external connection. I-V measurements were conducted  
41  
42 with Keithley 4200 Semiconductor Characterization System.  
43  
44

45 ASSOCIATED CONTENT

### 46 47 **Supporting Information**

48  
49 The HAADF TEM images, the setup of SHG, piezoelectricity measurements with devices are  
50  
51 given in this section. This material is available free of charge via the Internet.  
52  
53  
54

55  
56 AUTHOR INFORMATION

## Notes

<sup>†</sup>Y. Zhou and D. Wu contributed equally to this work.

The authors declare no competing financial interest.

## Corresponding Authors

\*Email: hlpeng@pku.edu.cn; kejilai@physics.utexas.edu

## ACKNOWLEDGEMENTS

The PFM work is supported by the Welch Foundation Grant F-1814. D.W. and Z.C. also acknowledges the support from NSF EFRI under Award # EFMA-1542747. The SHG work (Y. C. and M. C. D.) is supported by Welch Grant F-1038. The sample synthesis and device fabrication work are supported by the National Basic Research Program of China (No. 2014CB932500) and the National Natural Science Foundation of China (No. 21525310).

## Reference

- (1) Castro Neto, A. H.; Guinea, F.; Peres, N. M. R.; Novoselov, K. S.; Geim, A. K. *Rev. Mod. Phys.* **2009**, 81, 109-162.
- (2) Wang, Q. H.; Kalantar-Zadeh, K.; Kis, A.; Coleman, J. N.; Strano, M. S. *Nat. Nanotechnol.* **2012**, 7, 699-712.
- (3) Huang, B.; Clark, G.; Navarro-Moratalla, E.; Klein, D. R.; Cheng, R.; Seyler, K. L.; Zhong, D.; Schmidgall, E.; McGuire, M. A.; Cobden, D. H. *arXiv preprint arXiv:1703.05892* **2017**.
- (4) Wang, Y.; Xu, N.; Li, D.; Zhu, J. *Adv. Funct. Mater.* **2017**, 1604134.
- (5) Zhou, Y.; Jang, H. J.; Woods, J. M.; Xie, Y. J.; Kumaravadivel, P.; Pan, G. A.; Liu, J. B.; Liu, Y. H.; Cahill, D. G.; Cha, J. J. *Adv. Funct. Mater.* **2017**, 27.
- (6) Jones, A. M.; Yu, H. Y.; Ghimire, N. J.; Wu, S. F.; Aivazian, G.; Ross, J. S.; Zhao, B.; Yan, J. Q.; Mandrus, D. G.; Xiao, D.; Yao, W.; Xu, X. D. *Nat. Nanotechnol.* **2013**, 8, 634-638.
- (7) Mak, K. F.; Shan, J. *Nat. Photonics* **2016**, 10, 216-226.
- (8) Scott, J. F. *Ferroelectrics* **2000**, 236, 247-258.
- (9) Stengel, M.; Spaldin, N. A. *Nature* **2006**, 443, 679-682.

- 1  
2  
3  
4 (10) Crawley, E. F.; Deluis, J. *Aiaa J.* **1987**, 25, 1373-1385.
- 5  
6 (11) Wang, X. D.; Zhou, J.; Song, J. H.; Liu, J.; Xu, N. S.; Wang, Z. L. *Nano Lett.* **2006**, 6, 2768-  
7 2772.
- 8  
9 (12) Duerloo, K. A. N.; Ong, M. T.; Reed, E. J. *J. Phys. Chem. Lett.* **2012**, 3, 2871-2876.
- 10  
11 (13) Wu, W. Z.; Wang, L.; Li, Y. L.; Zhang, F.; Lin, L.; Niu, S. M.; Chenet, D.; Zhang, X.; Hao,  
12 Y. F.; Heinz, T. F.; Hone, J.; Wang, Z. L. *Nature* **2014**, 514, 470-474.
- 13  
14 (14) Zhu, H. Y.; Wang, Y.; Xiao, J.; Liu, M.; Xiong, S. M.; Wong, Z. J.; Ye, Z. L.; Ye, Y.; Yin,  
15 X. B.; Zhang, X. *Nat. Nanotechnol.* **2015**, 10, 151-155.
- 16  
17 (15) Chang, K.; Liu, J. W.; Lin, H. C.; Wang, N.; Zhao, K.; Zhang, A. M.; Jin, F.; Zhong, Y.; Hu,  
18 X. P.; Duan, W. H.; Zhang, Q. M.; Fu, L.; Xue, Q. K.; Chen, X.; Ji, S. H. *Science* **2016**, 353,  
19 274-278.
- 20  
21 (16) Fei, R. X.; Kang, W.; Yang, L. *Phys. Rev. Lett.* **2016**, 117, 097601.
- 22  
23 (17) Wang, H.; Qian, X. F. *2d Materials* **2017**, 4, 015042.
- 24  
25 (18) Belianinov, A.; He, Q.; Dziaugys, A.; Maksymovych, P.; Eliseev, E.; Borisevich, A.;  
26 Morozovska, A.; Banys, J.; Vysochanskii, Y.; Kalinin, S. V. *Nano Lett.* **2015**, 15, 3808-3814.
- 27  
28 (19) Susner, M. A.; Belianinov, A.; Borisevich, A.; He, Q.; Chyasnavichyus, M.; Demir, H.;  
29 Sholl, D. S.; Ganesh, P.; Abernathy, D. L.; McGuire, M. A.; Maksymovych, P. *Acs Nano* **2015**, 9,  
30 12365-12373.
- 31  
32 (20) Chyasnavichyus, M.; Susner, M. A.; Ievlev, A. V.; Eliseev, E. A.; Kalinin, S. V.; Balke, N.;  
33 Morozovska, A. N.; McGuire, M. A.; Maksymovych, P. *Appl. Phys. Lett.* **2016**, 109, 172901.
- 34  
35 (21) Liu, F. C.; You, L.; Seyler, K. L.; Li, X. B.; Yu, P.; Lin, J. H.; Wang, X. W.; Zhou, J. D.;  
36 Wang, H.; He, H. Y.; Pantelides, S. T.; Zhou, W.; Sharma, P.; Xu, X. D.; Ajayan, P. M.; Wang, J.  
37 L.; Liu, Z. *Nat. Commun.* **2016**, 7, 12357.
- 38  
39 (22) Butler, K. T.; Frost, J. M.; Walsh, A. *Energy & Environmental Science* **2015**, 8, 838-848.
- 40  
41 (23) Morris, M. R.; Pendlebury, S. R.; Hong, J.; Dunn, S.; Durrant, J. R. *Adv. Mater.* **2016**, 28,  
42 7123-7128.
- 43  
44 (24) Geim, A. K.; Grigorieva, I. V. *Nature* **2013**, 499, 419-425.
- 45  
46 (25) Grinberg, I.; West, D. V.; Torres, M.; Gou, G. Y.; Stein, D. M.; Wu, L. Y.; Chen, G. N.;  
47 Gallo, E. M.; Akbashev, A. R.; Davies, P. K.; Spanier, J. E.; Rappe, A. M. *Nature* **2013**, 503,  
48 509-512.
- 49  
50  
51  
52  
53  
54  
55  
56  
57  
58  
59  
60

- 1  
2  
3  
4  
5  
6  
7  
8  
9  
10  
11  
12  
13  
14  
15  
16  
17  
18  
19  
20  
21  
22  
23  
24  
25  
26  
27  
28  
29  
30  
31  
32  
33  
34  
35  
36  
37  
38  
39  
40  
41  
42  
43  
44  
45  
46  
47  
48  
49  
50  
51  
52  
53  
54  
55  
56  
57  
58  
59  
60
- (26) Ding, W.; Zhu, J.; Wang, Z.; Gao, Y.; Xiao, D.; Gu, Y.; Zhang, Z.; Zhu, W. *Nat. Commun.* **2017**, *8*, 14956.
- (27) Lee, H.; Kang, D. H.; Tran, L. *Mater. Sci. Eng. B-solid* **2005**, *119*, 196-201.
- (28) Han, G.; Chen, Z. G.; Drennan, J.; Zou, J. *Small* **2014**, *10*, 2747-2765.
- (29) Lai, K. J.; Peng, H. L.; Kundhikanjana, W.; Schoen, D. T.; Xie, C.; Meister, S.; Cui, Y.; Kelly, M. A.; Shen, Z. X. *Nano Lett.* **2009**, *9*, 1265-1269.
- (30) Tao, X.; Gu, Y. *Nano Lett.* **2013**, *13*, 3501-3505.
- (31) Lewandowska, R.; Bacewicz, R.; Filipowicz, J.; Paszkowicz, W. *Mater. Res. Bull.* **2001**, *36*, 2577-2583.
- (32) Lin, M.; Wu, D.; Zhou, Y.; Huang, W.; Jiang, W.; Zheng, W. S.; Zhao, S. L.; Jin, C. H.; Guo, Y. F.; Peng, H. L.; Liu, Z. F. *J. Am. Chem. Soc.* **2013**, *135*, 13274-13277.
- (33) Wu, D.; Pak, A. J.; Liu, Y. N.; Zhou, Y.; Wu, X. Y.; Zhu, Y. H.; Lin, M.; Han, Y.; Ren, Y.; Peng, H. L.; Tsai, Y. H.; Hwang, G. S.; Lai, K. J. *Nano Lett.* **2015**, *15*, 8136-8140.
- (34) Zhao, J. G.; Yang, L. X. *J. Phys. Chem. C* **2014**, *118*, 5445-5452.
- (35) Popovic, S.; Tonejc, A.; Grzetaplenkovic, B.; Celustka, B.; Trojko, R. *J. Appl. Crystallogr.* **1979**, *12*, 416-420.
- (36) Boyd, R. W., *Nonlinear optics*. 1992.
- (37) Li, Y. L.; Rao, Y.; Mak, K. F.; You, Y. M.; Wang, S. Y.; Dean, C. R.; Heinz, T. F. *Nano Lett.* **2013**, *13*, 3329-3333.
- (38) Kumar, N.; Najmaei, S.; Cui, Q. N.; Ceballos, F.; Ajayan, P. M.; Lou, J.; Zhao, H. *Phys. Rev. B* **2013**, *87*, 161403.
- (39) Balakrishnan, N.; Staddon, C. R.; Smith, E. F.; Stec, J.; Gay, D.; Mudd, G. W.; Makarovskiy, O.; Kudrynskiy, Z. R.; Kovalyuk, Z. D.; Eaves, L. *2D Mater* **2016**, *3*, 025030.
- (40) Dawber, M.; Rabe, K. M.; Scott, J. F. *Rev. Mod. Phys.* **2005**, *77*, 1083-1130.
- (41) Hong, S. S.; Cha, J. J.; Kong, D. S.; Cui, Y. *Nat. Commun.* **2012**, *3*, 757.
- (42) Chang, C. Z.; Zhang, J. S.; Feng, X.; Shen, J.; Zhang, Z. C.; Guo, M. H.; Li, K.; Ou, Y. B.; Wei, P.; Wang, L. L.; Ji, Z. Q.; Feng, Y.; Ji, S. H.; Chen, X.; Jia, J. F.; Dai, X.; Fang, Z.; Zhang, S. C.; He, K.; Wang, Y. Y.; Lu, L.; Ma, X. C.; Xue, Q. K. *Science* **2013**, *340*, 167-170.
- (43) Wen, X. N.; Wu, W. Z.; Ding, Y.; Wang, Z. L. *Adv. Mater.* **2013**, *25*, 3371-3379.

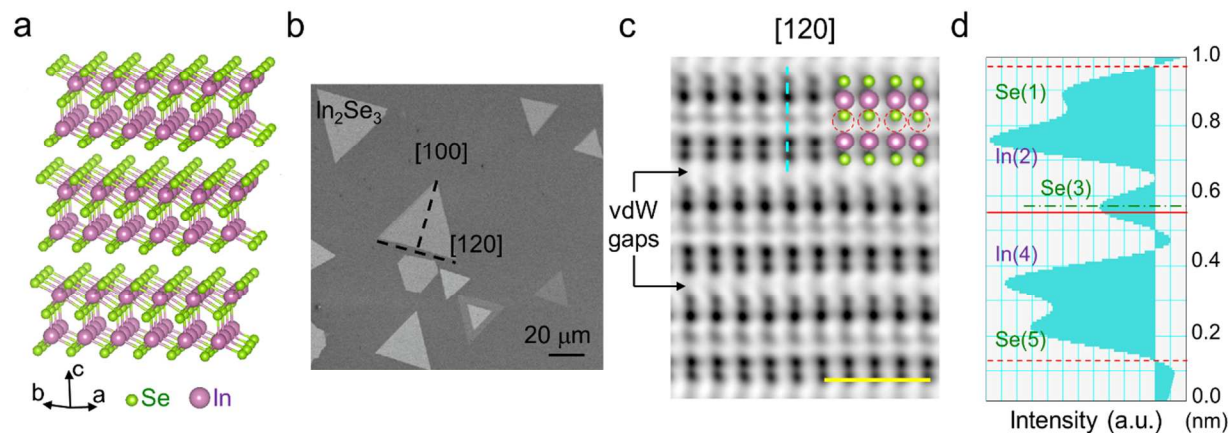


**Figure 1. Atomic structure of layered  $\text{In}_2\text{Se}_3$  nano-flake.** (a) Crystal structure of  $\alpha$ - $\text{In}_2\text{Se}_3$  in space group of R3m. (b) Scanning electron micrograph (SEM) of VPD grown  $\text{In}_2\text{Se}_3$  flakes. The [120] and [100] zone axes, along which the flakes are cut for STEM studies, are labeled in the image. (c) Cross-sectional annular bright-field (ABF) STEM image of an  $\text{In}_2\text{Se}_3$  flake cut along the [120] direction. Se and In atoms, as well as the van der Waals gaps, are indicated in the figure. The scale bar is 1 nm. (d) Intensity profile along the blue dashed line in (c). The center of the Se(3) atom is slightly shifted with respect to the central position of the quintuple layer.

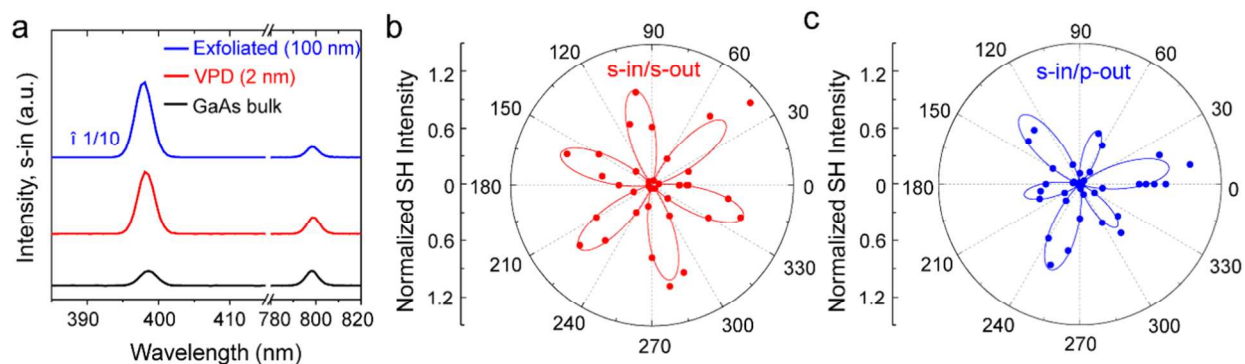


**Figure 2. SHG of  $\text{In}_2\text{Se}_3$  nano-flakes.** (a) SH spectral intensity at 399 nm (all polarizations) generated in reflection from VPD grown (red), exfoliated (blue)  $\text{In}_2\text{Se}_3$  flakes ( $\sim 100$  nm thick) and GaAs bulk. All samples are excited by equally intense s-polarized laser pulses with a wavelength of  $\lambda_{\text{ex}} = 798$  nm, which is strongly suppressed in the plot with respect to the corresponding SH peak. (b) Dependence of SHG signals on sample azimuthal angle  $\theta$  in the s-in/s-out configuration. The red curve is a fit to  $I = I_0 \cos^2(3\theta)$ . (c)  $\theta$ -dependence of SHG signals in the s-in/p-out configuration. The blue curve is a fit to  $I = I_0 (A + B \cdot \cos(3\theta))^2$ . The left-hand axes in (b) and (c) denote the radial scale.

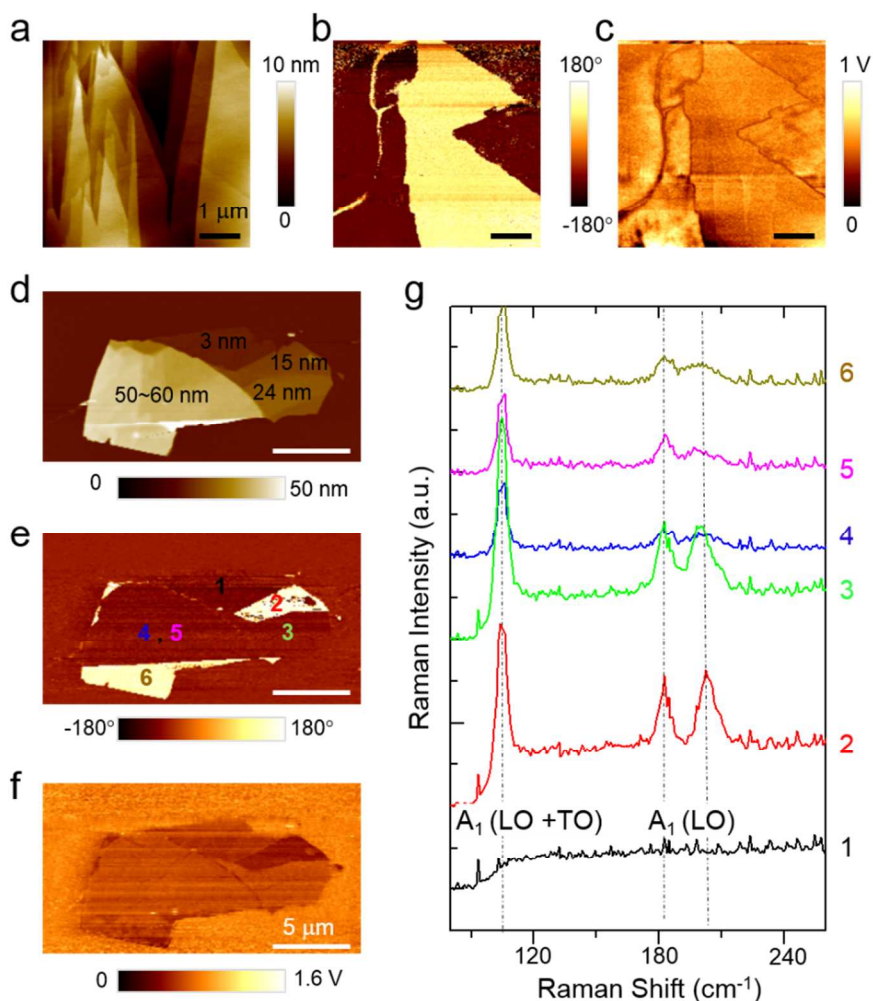


**Figure 3| Ferroelectric domains of  $\alpha$ - $\text{In}_2\text{Se}_3$  flakes.** (a - c) AFM, PFM phase and amplitude images of a thin  $\alpha$ - $\text{In}_2\text{Se}_3$  flake (> 100 nm). (d - f) AFM, PFM phase and amplitude images of a thin  $\alpha$ - $\text{In}_2\text{Se}_3$  flake exfoliated onto gold surface. The PFM phase contrast of  $180^\circ$  in both samples indicates the presence of different domains with opposite out-of-plane polarizations. The scale bars are 1  $\mu\text{m}$  in (a - c) and 5  $\mu\text{m}$  in (d - f). (g) Raman spectra at different locations labeled in (d). The prominent Raman peaks at  $104 \text{ cm}^{-1}$  and  $182 / 203 \text{ cm}^{-1}$  are associated with  $A(\text{LO} + \text{TO})$  and  $A(\text{LO})$  modes, respectively.



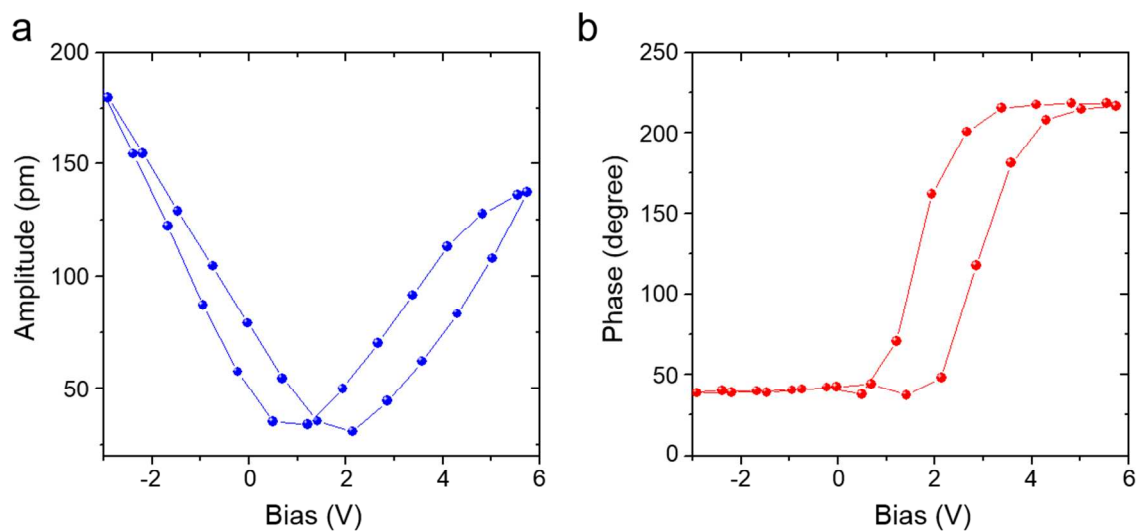


**Figure 4| Polarization reversal under external electrical field. On-field (a) PFM amplitude and (b) PFM phase hysteresis loops on a 20-nm-thick flake.**

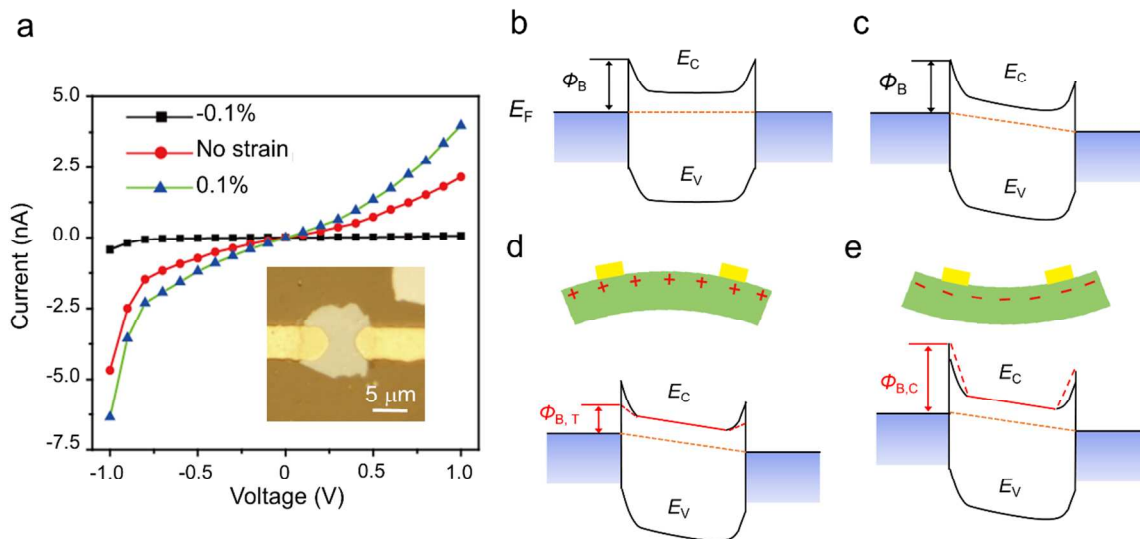


**Figure 5. Piezotronic effect on prototypical In<sub>2</sub>Se<sub>3</sub> devices.** (a) Typical I-V characteristics of two-terminal In<sub>2</sub>Se<sub>3</sub> devices under compressive (black), zero (red), and tensile (blue) strains by bending the substrate. Inset shows an image of typical 2D In<sub>2</sub>Se<sub>3</sub> device. (b - e) Band diagrams under different conditions: (b) Zero strain with zero source-drain bias. (c) Zero strain with non-zero source-drain bias. (d) Tensile strain with non-zero source-drain bias, resulting in lower Schottky barriers ( $\Phi_{B, T}$ ) and enhanced current. (e) Compressive strain with non-zero source-drain bias, resulting in higher Schottky barriers ( $\Phi_{B, C}$ ) and reduced current.